ACS APPLIED MATERIALS & INTERFACES

Forum Article

www.acsami.org

An Air-Stable DPP-thieno-TTF Copolymer for Single-Material Solar Cell Devices and Field Effect Transistors

Sasikumar Arumugam,[†] Diego Cortizo-Lacalle,[†] Stephan Rossbauer,[‡] Simon Hunter,[‡] Alexander L. Kanibolotsky,[†,§] Anto R. Inigo,*[,†] Paul A. Lane,[∥] Thomas D. Anthopoulos,*[,‡] and Peter J. Skabara*[,†]

[†]WestCHEM, Department of Pure and Applied Chemistry, University of Strathclyde, Glasgow G1 1XL, United Kingdom

[‡]Department of Physics & Centre for Plastic Electronics, Imperial College London, Exhibition Road, South Kensington, London SW7 2AZ, United Kingdom

[§]Institute of Physical−Organic Chemistry and Coal Chemistry, 83114 Donetsk, Ukraine

[∥]U.S. Naval Research Lab 4555 Overlook Ave., Washington, DC 20375, United States

Supporting Information

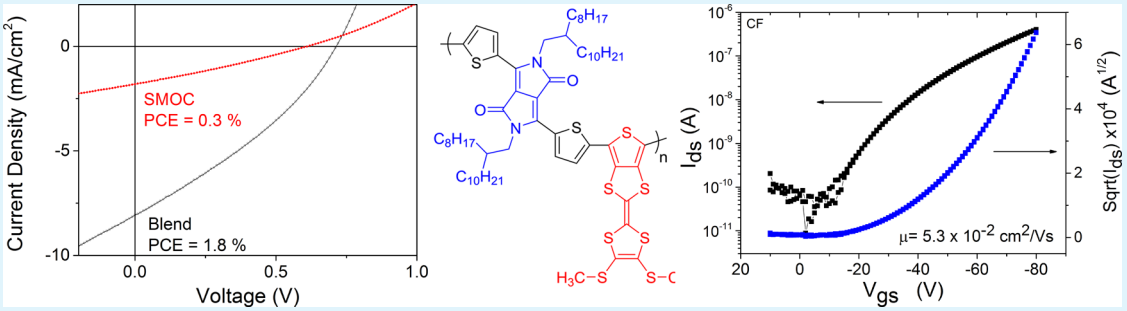

ABSTRACT: Following an approach developed in our group to incorporate tetrathiafulvalene (TTF) units into conjugated polymeric systems, we have studied a low band gap polymer incorporating TTF as a donor component. This polymer is based on a fused thieno-TTF unit that enables the direct incorporation of the TTF unit into the polymer, and a second comonomer based on the diketopyrrolopyrrole (DPP) molecule. These units represent a donor−acceptor copolymer system, p(DPP-TTF), showing strong absorption in the UV−visible region of the spectrum. An optimized p(DPP-TTF) polymer organic field effect transistor and a single material organic solar cell device showed excellent performance with a hole mobility of up to 5.3×10^{-2} $cm^2/(V\ s)$ and a power conversion efficiency (PCE) of 0.3%, respectively. Bulk heterojunction organic photovoltaic devices of p(DPP-TTF) blended with phenyl-C_{71}-butyric acid methyl ester ($PC_{71}BM$) exhibited a PCE of 1.8%.

KEYWORDS: *DPP-TTF polymer, OPV, OFET, single material OPV, hole mobility*

1. INTRODUCTION

The performance of organic electronic materials depends largely on the structure of the molecules or polymers, the device structure and the conditions used in the fabrication of the devices. Over the last two decades, a vast number of conjugated materials have been synthesized and characterized (single molecules, oligomers, dendrimers, and polymers). These compounds have been extensively tested in different devices such as organic photovoltaics (OPVs),[1−3] organic field-effect transistors (OFETs),[4−6] organic light-emitting diodes (OLEDs),[7,8] and electrochromic devices.[9] The synthesis and development of new families of materials are key activities in the field of organic electronics, but it is equally important to optimize materials processing conditions to obtain the best device characteristics. There are also other important considerations for ideal materials: a low band gap semiconductor to harvest light efficiently, adequate solubility, high stability, and matching hole/electron mobilities for donor and acceptor materials.[10] The latter is highly influenced by the nanomorphology that the materials adopt in the bulk. Therefore, a fine control of the film-forming property and desired morphology (e.g., bulk dimensionality, crystallinity)[11] is of high importance. Poly(3-hexyl-thiophene) (P3HT) is one of the classic examples in which vast amount of research and development work were carried out to understand the importance of fine synthetic control, morphology and device fabrication for optimized device performance. The simple parent polymer, polythiophene, bearing no substituents is not processable, and this fact led to the incorporation of alkyl

Special Issue: Advances towards Electronic Applications in Organic Materials

Received: December 3, 2014
Accepted: March 23, 2015
Published: April 2, 2015

DOI: 10.1021/am5080562
ACS Appl. Mater. Interfaces 2015, 7, 27999−28005

chains to obtain polymers soluble in common organic solvents.[12] In 1992, McCullough et al.[13] and Rieke et al.,[14] synthesized highly regioregular P3HT. In comparison to the amorphous regiorandom P3HT, self-organized and crystalline regioregular P3HT showed a significant increase in the conductivity. The relative simplicity in the synthesis of regioregular P3HT, along with its stability, has led to this material being one of the most studied systems in organic electronics. Despite some inherent drawbacks (the band gap of 1.7 eV is at the upper limit of the ideal value),[15] organic solar cells incorporating regioregular P3HT in combination with phenyl-C_{61}-butyric acid methyl ester ($PC_{61}BM$) have achieved power conversion efficiency of 0.8% for unannealed and 5% for annealed films.[16] These values have been obtained after significant efforts toward device optimization, by perfecting the fabrication conditions of the devices (e.g., donor/acceptor blend ratio, solvent choice, thermal annealing). It is clear from these examples that the optimization of the morphology of bulk heterojunction (BHJ) devices is crucial for highly efficient devices.

In our group, we developed a methodology for the synthesis of a thieno-TTF fused heterocyclic system that can be directly incorporated into a conjugated polymer backbone through the functionalized thiophene ring.[17,18] Recently, we published the synthesis of the novel conjugated polymer p(DPP-TTF; Figure 1) with electron donor thieno-TTF and electron acceptor

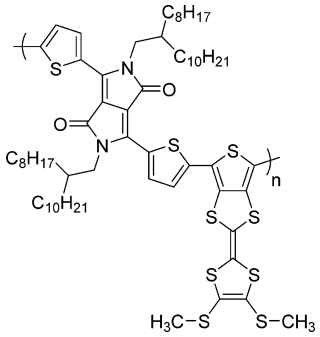

Figure 1. Chemical structure of the diketopyrrolopyrrole-tetrathiafulvalene polymer, p(DPP-TTF).

diketopyrrolopyrrole (DPP) units within the conjugated backbone and reported its performance in OFETs under ambient conditions. Optical, thermal, and electrochemical properties as well as the nanomorphology of this polymer indicated that it is a promising material for OFET and OPV applications.[11] Here, we report a more in-depth study of the material's performance in solar cells and its optical characteristics. In particular, we have found a remarkable power conversion efficiency for the single material organic solar cell (SMOC) with p(DPP-TTF) as the sole semiconductor material. These values are comparable to those fabricated from donor/acceptor SMOCs.[19] Recently, a SMOC fabricated from a copolymer consisting of P3HT and C_{60} repeat units gave an efficiency of 1.70% and short circuit current density (J_{sc}) of 6.15 mA/cm^2, and these values are the highest reported so far for a SMOC.[20] We have also investigated the charge carrier transport properties of the material processed under various conditions and resulting in different morphologies, using OFET characterization and AFM microscopy.

2. EXPERIMENTAL DETAILS AND CHARACTERIZATION

Acetone and chlorobenzene (CB), pentafluorobenzenethiol (PFBT), and octadecyltrichlorosilane (ODTS) were purchased from Sigma-Aldrich, Ltd. poly(ethylenedioxythiophene)/poly(styrenesulfonate) (PEDOT/PSS; Clevios P VP AI 4083) was purchase from Heraeus-Clevios. Two sets of samples were fabricated in which one set was fabricated with top-gate (TG)/bottom-contact configuration using Cytop as an insulator. Gold source and drain electrodes (70 nm) were deposited by high vacuum thermal evaporation on top of the silicon substrate using a shadow mask of channel length (L) of 40 μm and a channel width (W) of 1500 μm. Polymer p(DPP-TTF) was dissolved in chloroform (CF) and CB separately (12 mg/mL) and then spin coated at 1000 rpm and annealed at 200 °C for 30 min. Cytop was then spin cast at 2000 rpm for 60 seconds and annealed at 100 °C for 30 min. These samples were then placed in the evaporator chamber for deposition of aluminum (70 nm) as the gate electrode. The resulting OFET was then characterized. Another set of devices with bottom-gate (BG)/bottom-contact geometry was fabricated. Commercially available (Fraunhofer Institute) n-doped silicon chips with 200 nm of thermally grown SiO_2 with prefabricated interdigitated Au fingers having channel length of 10 μm, width of 1 cm, and capacitance per unit area of 1.7×10^{-8} F/cm^2 were used as substrates. The gold and SiO_2 surfaces were treated with PFBT and ODTS to form a SAM layer to reduce contact resistance and provide a favorable morphology for charge transport in the channel. A layer of p(DPP-TTF) was deposited on top of the PFBT and ODTS treated substrate by spin coating a polymer solution in chloroform (CF) (12 mg/mL) at a speed of 1000 rpm for 60 s. The polymer film was annealed on a hot plate at 200 °C under nitrogen atmosphere and finally the devices were subjected to electrical characterization under ambient conditions. The electrical characteristics of the FETs were measured using a Keithley 4200 source/measure unit. A tapping mode atomic force microscope from Digital Instruments 3100 was used to examine the surface morphologies of the semiconductors. The carrier mobility was calculated in the saturation regime from the slope plotting the square root of the drain current versus gate voltage (V_G) using the following equation:

$$\mu_{sat} = \frac{2L}{WC_i} \times \left(\frac{\partial\sqrt{I_{ds}}}{\partial V_g}\right)^2$$

where I_{ds} is the drain current, μ is the carrier mobility, V_g is the gate voltage, L is the channel length, W is the channel width, and C is the capacitance per unit area of an insulator material. The calculations in the linear regime were carried out using the following equation:

$$\mu_{lin} = \frac{\partial I_{ds,lin}}{\partial V_g} \times \frac{L}{WC_iV_d}$$

The OPV devices were fabricated with a conventional structure of glass/ITO/PEDOT−PSS/p(DPP-TTF)−$PC_{71}BM$/Ca(40 nm)/Al(40 nm), using a solution process for depositing a hole-collecting layer and donor−acceptor blend. The 100 nm thick layer of ITO-coated glass substrates were cleaned by ultrasonic treatment in acetone and isopropyl alcohol for 5 min and dried by a stream of nitrogen. A thin hole-collecting layer of PEDOT−PSS was spin coated at 4000 rpm on the ITO/glass substrate. After baking at 120 °C for 20 min, the substrates were transferred into a nitrogen-filled glovebox and the rest of the OPV device processing and characterizations were carried out in the glovebox. The donor−acceptor BHJ devices with different blend ratios were prepared in CF or *o*-dichlorobenzene (*o*-DCB) solutions and stirred for 12 h before spin coating at 800 rpm. Finally, a 40 nm calcium layer and a 40 nm aluminum layer were deposited on the active layer under high vacuum (2×10^{-6} mbar). The effective area of each cell (4×1.5 mm) was defined by the shadow mask. The current density−voltage (I−V) curves of photovoltaic devices were obtained by a Keithley 4200 source/measure unit. The photocurrent was measured under AM 1.5 (100 mW/cm^2) irradiation using a Newport

DOI: 10.1021/am5080562
ACS Appl. Mater. Interfaces 2015, 7, 27999−28005

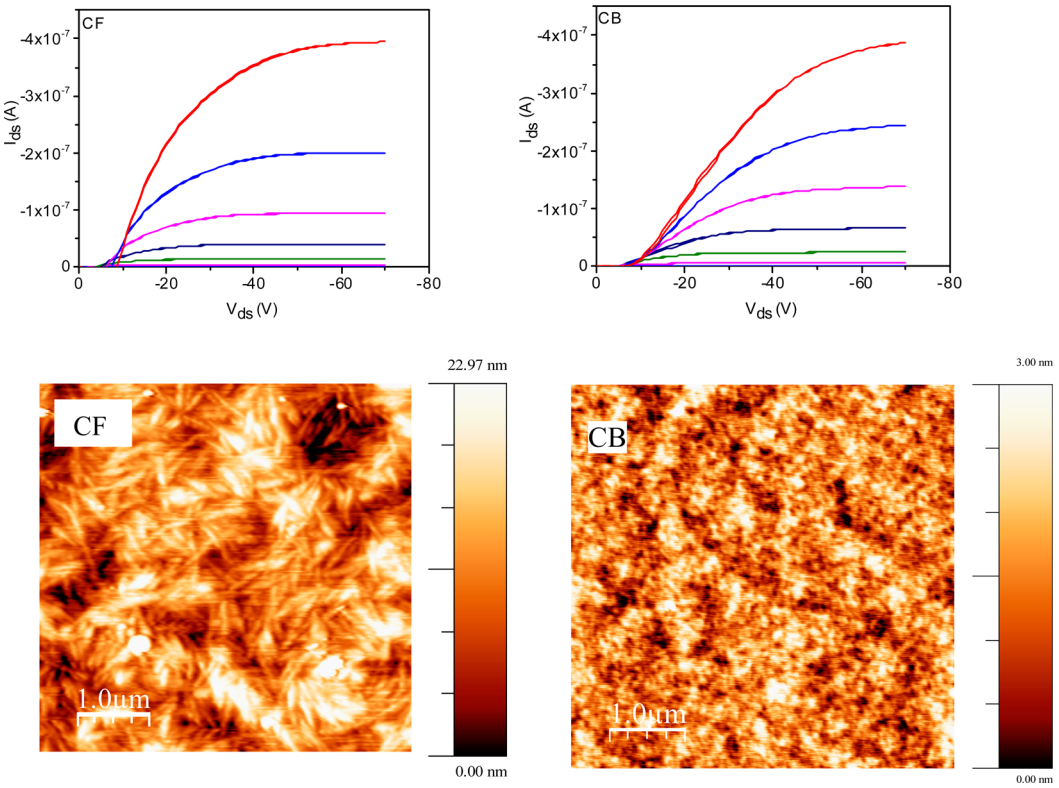

Figure 2. Output characteristics and AFM images of OFETs fabricated by spin coating of p(DPP-TTF) from CF and CB solutions. Measurements were performed at gate voltage intervals of 10 V from 0 to −80 V in a top-gate device configuration.

Table 1. OFET Performance for Devices of Various Configurations Fabricated Using Different Solvents on Si/SiO_2 Substrate

	geometry	capacitance per unit area, F/cm^2	solvent used	V_{gs} interval range, V	V_{ds}, V	on/off ratio	μ, $cm^2/(V\ s)$	V_T,V
A	TG/CYTOP	2.1×10^{-10}	CB	−50 to −80 (sat)	−70	10^4	3.8×10^{-2}	−30
				−40 to −65 (lin)	−20	10^4	1.2×10^{-2}	−20
B	TG/CYTOP	2.1×10^{-10}	CF	−50 to −80 (sat)	−70	10^4	5.3×10^{-2}	−38
				−60 to -80 (lin)	−15	10^4	3.8×10^{-2}	−40
C	BG/ODTS	1.7×10^{-8}	CF	−30 to −58 (forward)	−50	10^4	7.3×10^{-3}	−8.6
				−50 to −80 (reverse)			2.0×10^{-2}	−39

solar simulator, calibrated with a standard Si solar cell. The efficiency of the solar cell was calculated by the following equation:

$$\eta_{max} = \frac{V_{OC} I_{SC} FF}{P_{in}}$$

where V_{oc} is the open-circuit voltage, J_{sc} is the short circuit current density and FF is the fill factor. Incident photon conversion efficiency (IPCE) spectra were measured with the device under bias illumination by a white light source and using a calibrated, tunable light source.

3. RESULTS AND DISCUSSION

Figure 2 shows the output characteristics for p(DPP-TTF) devices fabricated from CF and CB solutions separately and measured at different gate voltages up to −80 V at intervals of −10 V. Figure SI1 (Supporting Infomation) shows the transfer characteristics of an OFET device with a thin film of p(DPP-TTF) annealed at 200 °C for half an hour. Devices A and B were fabricated using a top-gate (TG) configuration and Cytop as an insulator, while device C was constructed using SiO_2/ODTS as the gate dielectric with a bottom-gate (BG) structure, as listed in Table 1. We also attempted electron mobility measurements by using a low work function metal, such as calcium, as source and drain electrodes, but we did not observe any output or transfer characteristics with reasonable quality to deduce the electron mobility. At this point, we are confident that this material does not exhibit ambipolar mobility. Due to the presence of the strongly electron-rich TTF unit, it is not a surprise that the material does not show any n-type behavior. Detrimental n-type materials interactions are revealed by comparing HOMO and LUMO levels of the polymer in solution and solid state. As was reported before,[11] the polymer in the solid film has a deeper highest occupied molecular orbital (HOMO; 5.13 eV) and a slightly more shallow lowest unoccupied molecular orbital (LUMO) level (3.49 eV) than in solution (HOMO of 4.95 eV and LUMO of 3.55 eV), which provides evidence of some interaction between donor and acceptor sites in the solid. To gain a better understanding of the effect of morphology on the charge carrier mobility, atomic force microscopy (AFM) has been utilized to describe the distinctive features of the polymer.

Tapping mode AFM images (Figure 2) were recorded on the same devices used for OFET measurements. The AFM images showed that the film formed from CB consisted of closely packed grain-like structures with small domain sizes and flat surfaces (rms of 0.53 nm). This type of morphology is due to the strong propensity of p(DPP-TTF) to aggregate when spun

DOI: 10.1021/am5080562
ACS Appl. Mater. Interfaces 2015, 7, 27999−28005

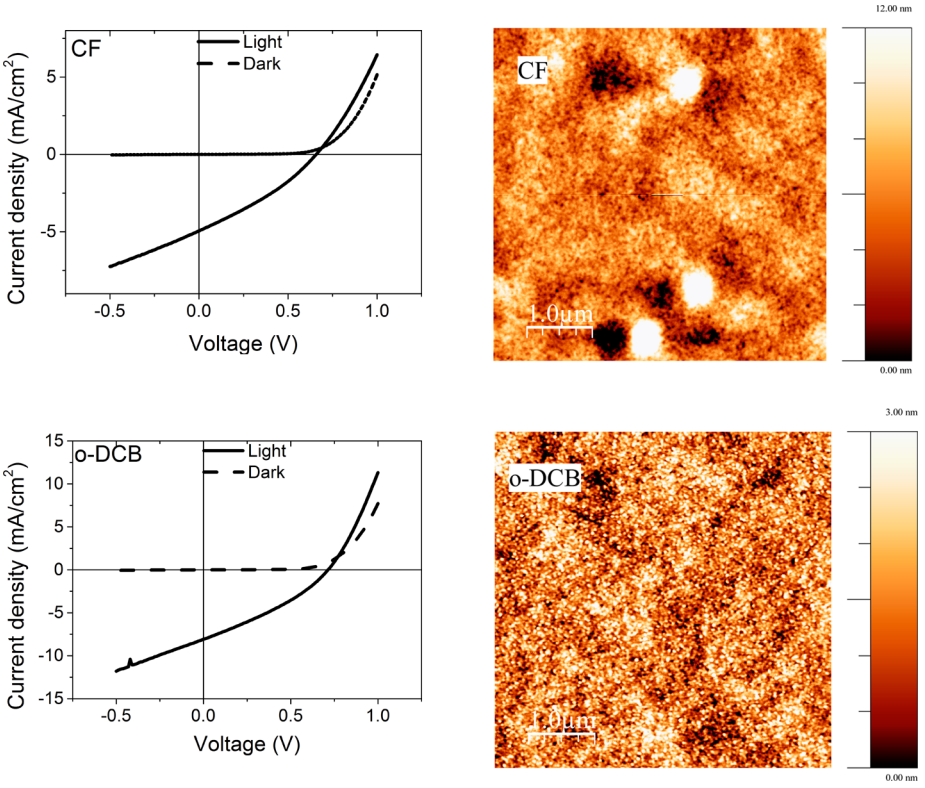

Figure 3. *I*−*V* curves and AFM images of solar cells fabricated by spin coating a p(DPP-TTF):$PC_{71}BM$ (1:4) blend from CF and *o*-DCB solutions after annealing at 120 °C for 20 min.

from this solvent. Upon annealing the rate of grain nucleation is higher than the rate of growth, which produces small crystalline domains. Previously, a similar tight-grain packing morphology was observed in the case of poly(2,5-bis(3-hexadecylthiophen-2-yl)thieno[3,2-*b*]thiophene, which proved to be beneficial for good charge transport in OFETs.[21] For this type of morphology, the top-gate OFET device gave a hole mobility of 3.8×10^{-2} $cm^2/(V\ s)$ in the saturation regime and 1.2×10^{-2} $cm^2/(V\ s)$ in the linear regime (Table 1).

The morphology of the thin film spin coated from CF solution is different. The energy of solvation in this solvent should be higher than that in CB due to the interaction of the polarized C−H bond of the solvent molecules with TTF and with the lone pairs of the DPP carbonyl oxygen atoms. This will prevent quick formation of the aggregate, so the rate of nucleation in this case is going to be lower than the rate of grain growth upon annealing. This leads to morphology in the film with a larger size of domain. In the case of CF, we obtained a higher mobility for the top-gate configuration of the OFET (5.3×10^{-2} $cm^2/(V\ s)$ in the saturation regime and 3.8×10^{-2} $cm^2/(V\ s)$ in the linear regime). Therefore, due to the relative stability of solvated states in the film, not only is a larger size of crystalline domain produced but a smoother grain boundary as well, which is confirmed by a low degree of roughness of the surface (rms of 4.5 nm; note that larger grains usually give a much higher degree of roughness, so that the comparison with the surface of the film derived from CB is less than anticipated). The bottom-gate configuration was attempted for an OFET fabricated by spin coating p(DPP-TTF) from CF, but the device exhibited inferior performance (Table 1).

The mobility and threshold voltage values derived from thin films of p(DPP-TTF) with a SiO_2 gate dielectric (Figure SI2, Supporting Infomation), were largely different when estimated from the forward and reverse sweeps because of a large hysteresis. The hysteresis gap (ΔV_T) is defined as the difference in threshold voltage between the backward and forward V_{gs} sweeps, as determined by the linear extrapolation method. The observed hysteresis is a current-increasing type, where I_{ds} was lower during the backward sweep of V_{gs} than I_{ds} during the forward sweep. It is frequently observed in the current−voltage (I−V) characteristics of organic semiconductor devices and can complicate the mobility extraction.[22] From the forward sweep the calculated mobility was 7.3×10^{-3} $cm^2/(V\ s)$ with a threshold voltage of −8.6 V. Conversely, from the reverse sweep, the mobility is increased more than 2-fold (2.0×10^{-2} $cm^2/(V\ s)$, with a V_T of −39 V), because of the higher drop of current on the backward sweep of V_{gs}. We list in Table 1 the calculated mobility and threshold voltage for both Cytop and SiO_2 gate dielectrics. Hysteresis showed on-to-off transfer curves shifted toward a higher V_{gs} (Figure SI2, Supporting Infomation) compared with off-to-on sweeps. There are two possible mechanisms that can link the sweep change with the current (I_{ds}) increase: (1) slow polarization of the gate dielectric, or (2) charge trapping and detrapping at the semiconductor/dielectric interface.[23,24] While attempting the treatment of an ODTS layer onto SiO_2 substrates, we observed that some of the ODTS material appears to be hydrolyzed and the hydroxyl groups at the dielectric interface appear to act as ionic impurities which are capable of slow polarization under applied voltage.[23] When the gate is swept from off-to-on, polar species in the dielectric medium are polarized at the interface between the semiconductor and the gate electrode. If the polarized species do not respond quickly to the changes in the gate electric field, they may remain polarized without being able to return to their original sites during the on-to-off gate sweep. As a result, the on-to-off transfer curve shifts to higher V_{gs}

DOI: 10.1021/am5080562
ACS Appl. Mater. Interfaces 2015, 7, 27999−28005

Table 2. Comparison of Device Characteristics for Solar Cells Fabricated Using Different Solvents and Annealed at 120°C[a]

active layer p(DPP-TTF):$PC_{71}BM$	solvent	J_{sc} (mA/cm^2)	V_{oc} (V)	FF	PCE (%)	R_S (Ω)	R_{Sh} (Ω)
1:4	CF	4.9	0.66	0.31	1.0	1320	3210
1:4	o-DCB	8.0	0.71	0.32	1.8	704	2209
1:0	o-DCB	1.8	0.61	0.28	0.3	4514	6796

[a] J_{sc} is the short circuit current density, V_{oc} is the open-circuit voltage, FF is the fill factor, and PCE is the overall power conversion efficiency.

values compared to the off-to-on sweep.[25] Slow polarization also artificially increases the capacitance of the gate dielectric, resulting in a large increase in I_{ds} and the overestimation of mobility. Recently, Gu et al.[23] and Kim et al.[26] found that in the case of pentacene-based OFETs containing ODTS modified SiO_2 dielectrics, the hysteresis observed during the full sweep of a gate is due to long-lived charge traps present at the interface between the semiconductor and the gate dielectric, where trapping and detrapping of holes and electrons take place under an applied gate voltage. The above explains that the extraction of mobility from both forward and reverse sweeps in the case of device C (Table 1) does not correspond to the field effect characteristic only. However, the complete absence of hysteresis in the case of devices A and B with Cytop as the gate dielectric may be due to the more hydrophobic nature of the cyclic fluoropolymer, rather than the SiO_2 gate dielectric properties. The performance of devices A and B highlights the advantage of the top-gate configuration where the channel is not affected by the possible impurities introduced by the chemical treatment of the substrate surface. Another advantage of Cytop as the choice of dielectric in devices A and B is its low permittivity. Although the higher dielectric constant of the gate insulator provides a greater degree of charge injection in the channel[27] using low permittivity polymers (Cytop) allows to avoid trap states by reducing energetic disorder. The hole mobility of p(DPP-TTF) might be improved by adjusting the structure of the polymer. A shorter branched alkyl substituent might be beneficial for increased π-stacking interactions and polymer crystallinity.[28]

Bulk heterojunction solar cells were fabricated from p(DPP-TTF):$PC_{71}BM$ using both *o*-DCB and CF as the solvents. The HOMO and LUMO levels of p(DPP-TTF) are 5.13 and 3.49 eV, respectively, which match well with those of the commonly used electron acceptor material, ($PC_{71}BM$, 4.1 eV). A ratio of 1:4 was found to be optimum for device fabrication and performance. Figure 3 shows the OPV characteristics of p(DPP-TTF):$PC_{71}BM$ spin coated from CF. The device has a short circuit current density (J_{sc}) of 4.9 mA/cm^2, an open circuit voltage (V_{oc}) of 660 mV, and fill factor of 0.31, which result in a power conversion efficiency (PCE) of 1.0%. However, the devices prepared with *o*-DCB showed nearly a 2-fold increase in PCE over those spin coated from CF. These *o*-DCB devices (Figure 3) exhibited a fill factor of 0.32, a V_{oc} of 710 mV, an J_{sc} of 8 mA/cm^2, and PCE of 1.8%, as shown in Table 2. Absorption and incident photon conversion efficiency (IPCE) measurements demonstrate that the polymer both absorbs and generates photocurrent from near-infrared light. Figure 4 compares the absorption spectrum of p(DPP-TTF) and the external quantum efficiency (EQE) of a p(DPP-TTF) device, spin-cast from CF. The peak EQE is approximately 45%. The device has a good response throughout the visible and near-infrared spectrum, extending to a maximum wavelength of ca. 1050 nm. The stronger response of the device relative to the absorption spectrum of p(DPP-TTF) reflects contributions of the fullerene acceptor to the photocurrent.

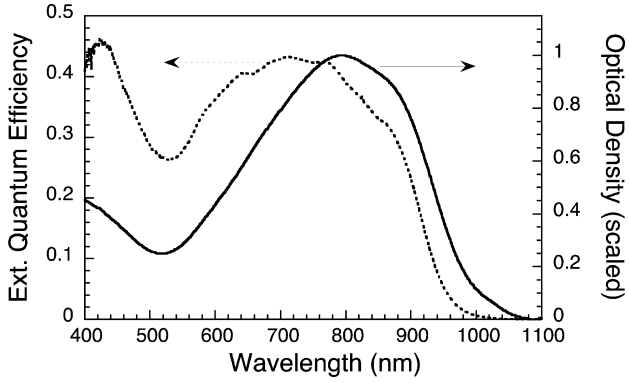

Figure 4. Absorption spectrum of p(DPP-TTF) (solid state, continuous line) and the IPCE spectrum (dotted line) of a p(DPP-TTF):$PC_{71}BM$ (1:4) blend solar cell, spin-cast from a CF solution. The absorption spectrum is normalized to the peak value.

Figure 3 shows the tapping mode AFM images of an OPV device fabricated by spin coating a p(DPP-TTF):$PC_{71}BM$(1:4) blend from CF solution. Annealing at 120 °C for 20 min gave a coarse surface morphology consisting of discontinuous film (dark areas) with a rms value of 2.3 nm. This can be a sign of increased demixing between p(DPP-TTF) and $PC_{71}BM$. On the contrary, the p(DPP-TTF):$PC_{71}BM$ film spin coated from *o*-DCB (Figure 3) exhibits a more homogeneous morphology (rms value of 0.7 nm). This structure could be achieved by more pronounced donor−acceptor interactions in *o*-DCB, which in turn would lead to a nanoscaled interpenetrating network and hence a higher PCE of 1.8%. As the blend ratio increases to 1:5 and 1:6, the p(DPP-TTF) and $PC_{71}BM$ components seem to segregate into larger domains, as observed in Figure SI3 (Supporting Infomation). These result in poor charge carrier transport in addition to a lower fill factor and open circuit voltage. The series resistance (R_s) and shunt resistance (R_{sh}) calculated from the *I*−*V* characteristics are shown in Table 2. These results indicate that the p(DPP-TTF):$PC_{71}BM$ film spin coated from *o*-DCB devices show nearly 2-fold lower R_s values when compared to those of the p(DPP-TTF):$PC_{71}BM$ film spin coated from CF devices. This significant decrease in series resistance is in line with better surface morphology, as shown in the corresponding AFM image (Figure 3), which can be attributed to solvent annealing. Even though the R_{sh} of *o*-DCB is lower than that of the CF devices, the ratio R_{sh}/R_s is higher compared to that of the CF devices. This higher value of R_{sh}/R_s in addition to an increase in J_{sc} in *o*-DCB devices would again indicate that the BHJ devices processed by *o*-DCB have a better interpenetrating morphology and lower surface roughness (as verified by the AFM images) and hence contribute to a higher efficiency.

SMOC devices of p(DPP-TTF) were prepared by spin coating from *o*-DCB, since bulk heterojunction solar cells fabricated from p(DPP-TTF):$PC_{71}BM$ in this solvent showed better performance than those made using CF. The devices were annealed at 120 °C for 20 min. The SMOC exhibited a

DOI: 10.1021/am5080562
ACS Appl. Mater. Interfaces 2015, 7, 27999−28005

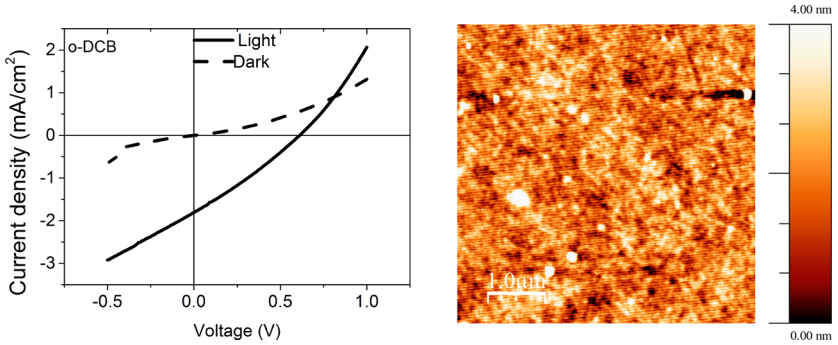

Figure 5. *I*−*V* characteristics and AFM for p(DPP-TTF) as a single component OPV of the pure polymer spin coated onto ITO/PEDOT:PSS substrates and annealed at 120 °C for 20 min.

power conversion efficiency of 0.3% with a J_{sc} of 1.8 mA/cm^2 and V_{oc} of 610 mV. The *I*−*V* characteristics of the device and the AFM image of the film are shown in Figure 5. The SMOC PCE is modest compared to those of the devices fabricated from donor−acceptor block copolymers,[29,30] due to poor charge separation and lack of electron mobility in the DPP-TTF copolymer. Nevertheless, the design of the DPP-TTF copolymer appears to be highly promising for SMOC applications and fully functionalized self-organizing molecular devices and molecular electronics in general.[31−33] To rationalize these findings, we investigated the semiconductor morphology of the thin films (Figure 5). Although the overall surface roughness is very low (rms of ca. 1.0 nm), there are larger particulate structures embedded into the uniform crystalline domains and pin holes. These defects are detrimental to charge carrier transport and will adversely affect the power conversion efficiency. The SMOC architecture provides 3 times higher R_{sh} compared to that of the BHJ devices processed from the same solvent, *o*-DCB (Table 2). This higher R_{sh} would suggest that the photogenerated charge carriers are separated and transported with no significant recombination across the SMOC device and toward the electrodes. However, there is also a relative increase in R_s, which could be due to the low mobility of the semiconductor toward electron transport and inefficient exciton dissociation. This increase in series resistance would also contribute to a lower fill factor and hence to an overall lower power efficiency.

4. CONCLUSION

In summary, we have demonstrated that the copolymer p(DPP-TTF), containing diketopyrrolopyrrole and tetrathiafulvalene units, is a high mobility semiconductor for organic thin film transistors and solar cells. The best solvent for the fabrication of OFETs has been found to be CF, which provides larger crystalline domains with smoother grain boundaries. This optimized device fabrication method provides the highest hole mobility of the devices studied here and, contrary to our previous work,[11] the devices demonstrate negligible hysteresis by the elimination of trap states.

For the first time, the TTF-containing polymer has been studied in photovoltaic devices. BHJ solar cells made from blends of p(DPP-TTF) and $PC_{71}BM$ provide modest power conversion efficiencies. Despite not exhibiting any noticeable field effect electron mobility, the semiconductor p(DPP-TTF) in a single material organic solar cell shows a PCE of 0.3%, which marks the polymer as a promising structure to develop for SMOCs. The lack of electron mobility from p(DPP-TTF) OFET devices is an obvious issue that can be addressed in the design of next-generation DPP-TTF polymer materials for higher power conversion efficiencies.

■ ASSOCIATED CONTENT

Supporting Information

This material is available free of charge via the Internet at http://pubs.acs.org.

■ AUTHOR INFORMATION

Corresponding Authors

*E-mail: anto.inigo@strath.ac.uk.
*E-mail: peter.skabara@strath.ac.uk.
*E-mail: thomas.anthopoulos@imperial.ac.uk.

Notes

The authors declare no competing financial interest.

■ ACKNOWLEDGMENTS

P.J.S. thanks the Royal Society for a Wolfson Research Merit Award. We also thank the EPSRC for funding under grant EP/J007005.

■ REFERENCES

(1) Facchetti, A. Π-Conjugated Polymers for Organic Electronics and Photovoltaic Cell Applications. *Chem. Mater.* **2010**, *23*, 733−758.
(2) Brédas, J. L.; Norton, J. E.; Cornil, J.; Coropceanu, V. Molecular Understanding of Organic Solar Cells: The Challenges. *Acc. Chem. Res.* **2009**, *42*, 1691−1699.
(3) Beaujuge, P. M.; Fréchet, J. M. J. Molecular Design and Ordering Effects in Π-Functional Materials for Transistor and Solar Cell Applications. *J. Am. Chem. Soc.* **2011**, *133*, 20009−20029.
(4) Yuen, J. D.; Wudl, F. Strong Acceptors in Donor-Acceptor Polymers for High Performance Thin Film Transistors. *Energy Environ. Sci.* **2013**, *6*, 392−406.
(5) Murphy, A. R.; Fréchet, J. M. J. Organic Semiconducting Oligomers for Use in Thin Film Transistors. *Chem. Rev.* **2007**, *107*, 1066−1096.
(6) Zaumseil, J.; Sirringhaus, H. Electron and Ambipolar Transport in Organic Field-Effect Transistors. *Chem. Rev.* **2007**, *107*, 1296−1323.
(7) Yook, K. S.; Lee, J. Y. Organic Materials for Deep Blue Phosphorescent Organic Light-Emitting Diodes. *Adv. Mater.* **2012**, *24*, 3169−3190.
(8) Sessolo, M.; Bolink, H. J. Hybrid Organic−Inorganic Light-Emitting Diodes. *Adv. Mater.* **2011**, *23*, 1829−1845.
(9) Gunbas, G.; Toppare, L. Electrochromic Conjugated Polyheterocycles and Derivatives-Highlights from the Last Decade Towards Realization of Long Lived Aspirations. *Chem. Commun.* **2012**, *48*, 1083−1101.
(10) Roman, L. S.; Andersson, M. R.; Yohannes, T.; Inganás, O. Photodiode Performance and Nanostructure of Polythiophene/C60 Blends. *Adv. Mater.* **1997**, *9*, 1164−1168.

DOI: 10.1021/am5080562
ACS Appl. Mater. Interfaces 2015, 7, 27999−28005

(11) Lacalle, D. C.; Arumugam, S.; Elmasly, S. E. T.; Kanibolotsky, A. L.; Findlay, N. J.; Inigo, A. R.; Skabara, P. J. Incorporation of Fused Tetrathiafulvalene Units in a DPP-Terthiophene Copolymer for Air Stable Solution Processable Organic Field Effect Transistors. *J. Mater. Chem.* **2012**, *22*, 11310−11315.
(12) Elsenbaumer, R. L.; Jen, K. Y.; Oboodi, R. Processible and Environmentally Stable Conducting Polymers. *Synth. Met.* **1986**, *15*, 169−174.
(13) McCullough, R. D.; Lowe, R. D. Enhanced Electrical Conductivity in Regioselectively Synthesized Poly(3-alkylthiophenes). *J. Chem. Soc., Chem. Commun.* **1992**, *0*, 70−72.
(14) Chen, T. A.; Rieke, R. D. The First Regioregular Head-to-Tail Poly(3-hexylthiophene-2,5-diyl) and a Regiorandom Isopolymer: Nickel Versus Palladium Catalysis of 2(5)-Bromo-5(2)-(bromozincio)-3-hexylthiophene Polymerization. *J. Am. Chem. Soc.* **1992**, *114*, 10087−10088.
(15) Kroon, R.; Lenes, M.; Hummelen, J. C.; Blom, P. W. M.; de Boer, B. Small Bandgap Polymers for Organic Solar Cells (Polymer Material Development in the Last 5 Years). *Polym. Rev.* **2008**, *48*, 531−582.
(16) Ma, W.; Yang, C.; Gong, X.; Lee, K.; Heeger, A. J. Thermally Stable, Efficient Polymer Solar Cells with Nanoscale Control of the Interpenetrating Network Morphology. *Adv. Funct. Mater.* **2005**, *15*, 1617−1622.
(17) Skabara, P. J.; Berridge, R.; McInnes, E. J. L.; West, D. P.; Coles, S. J.; Hursthouse, M. B.; Mullen, K. The Electroactivity of Tetrathiafulvalene vs Polythiophene: Synthesis and Characterisation of a Fused Thieno-TTF Polymer. *J. Mater. Chem.* **2004**, *14*, 1964−1969.
(18) Berridge, R.; Skabara, P. J.; Pozo-Gonzalo, C.; Kanibolotsky, A.; Lohr, J.; McDouall, J. J. W.; McInnes, E. J. L.; Wolowska, J.; Winder, C.; Sariciftci, N. S.; Harrington, R. W.; Clegg, W. Incorporation of Fused Tetrathiafulvalenes (TTFS) into Polythiophene Architectures: Varying the Electroactive Dominance of the TTF Species in Hybrid Systems. *J. Phys. Chem. B* **2006**, *110*, 3140−3152.
(19) Roncali, J. Single Material Solar Cells: The Next Frontier for Organic Photovoltaics? *Adv. Energy Mater.* **2011**, *1*, 147−160.
(20) Miyanishi, S.; Zhang, Y.; Tajima, K.; Hashimoto, K. Fullerene Attached All-Semiconducting Diblock Copolymers for Stable Single-Component Polymer Solar Cells. *Chem. Commun.* **2010**, *46*, 6723−6725.
(21) Chabinyc, M. L.; Lujan, R.; Endicott, F.; Toney, M. F.; McCulloch, I.; Heeney, M. Effects of the Surface Roughness of Plastic-Compatible Inorganic Dielectrics on Polymeric Thin Film Transistors. *Appl. Phys. Lett.* **2007**, *90*, 233503−233508.
(22) Ryu, K.; Kymissis, I.; Bulovic, V.; Sodini, C. G. Direct Extraction of Mobility in Pentacene Ofets Using *C*−*V* and *I*−*V* Measurements. *Elect. Dev. Lett. IEEE* **2005**, *26*, 716−718.
(23) Gu, G.; Kane, M. G.; Mau, S. C. Reversible Memory Effects and Acceptor States in Pentacene-Based Organic Thin-Film Transistors. *J. Appl. Phys.* **2007**, *101*, 014504.
(24) Gu, G.; Kane, M. G. Moisture Induced Electron Traps and Hysteresis in Pentacene-Based Organic Thin-Film Transistors. *Appl. Phys. Lett.* **2008**, *92*, 053305.
(25) Kim, S. H.; Yun, W. M.; Kwon, O. K.; Hong, K.; Yang, C.; Choi, W. S.; Park, C. E. Hysteresis Behaviour of Low-Voltage Organic Field-Effect Transistors Employing High Dielectric Constant Polymer Gate Dielectrics. *J. Phys. D: Appl. Phys.* **2010**, *43*, 456102.
(26) Kim, S. H.; Nam, S.; Jang, J.; Hong, K.; Yang, C.; Chung, D. S.; Park, C. E.; Choi, W. S. Effect of the Hydrophobicity and Thickness of Polymer Gate Dielectrics on the Hysteresis Behavior of Pentacene-Based Field-Effect Transistors. *J. Appl. Phys.* **2009**, *105*, 104509.
(27) Chen, F. C.; Chu, C. W.; He, J.; Yang, Y.; Lin, J. L. Organic Thin-Film Transistors with Nanocomposite Dielectric Gate Insulator. *Appl. Phys. Lett.* **2004**, *85*, 3295−3297.
(28) Yuan, J.; Huang, X.; Zhang, F.; Lu, J.; Zhai, Z.; Di, C.; Jiang, Z.; Ma, W. Design of Benzodithiophene-Diketopyrrolopyrrole Based Donor-Acceptor Copolymers for Efficient Organic Field Effect Transistors and Polymer Solar Cells. *J. Mater. Chem.* **2012**, *22*, 22734−22742.
(29) Zhang, Q.; Cirpan, A.; Russell, T. P.; Emrick, T. Donor−Acceptor Poly(Thiophene-Block-Perylene Diimide) Copolymers: Synthesis and Solar Cell Fabrication. *Macromolecules* **2009**, *42*, 1079−1082.
(30) Wang, J.; Higashihara, T. Synthesis of All-Conjugated Donor-Acceptor Block Copolymers and Their Application in All-Polymer Solar Cells. *Polym. Chem.* **2013**, *4*, 5518−5526.
(31) Lindner, S. M.; Hüttner, S.; Chiche, A.; Thelakkat, M.; Krausch, G. Charge Separation at Self-Assembled Nanostructured Bulk Interface in Block Copolymers. *Angew. Chem., Int. Ed.* **2006**, *45*, 3364−3368.
(32) Sommer, M.; Hüttner, S.; Steiner, U.; Thelakkat, M. Influence of Molecular Weight on the Solar Cell Performance of Double-Crystalline Donor-Acceptor Block Copolymers. *Appl. Phys. Lett.* **2009**, *95*, 183308−3.
(33) Walker, B.; Kim, C.; Nguyen, T. Q. Small Molecule Solution-Processed Bulk Heterojunction Solar Cells. *Chem. Mater.* **2010**, *23*, 470−482.

DOI: 10.1021/am5080562
ACS Appl. Mater. Interfaces 2015, 7, 27999−28005